BBA - Biomembranes 1861 (2019) 380–386

Contents lists available at ScienceDirect

BBA - Biomembranes

journal homepage: www.elsevier.com/locate/bbamem

Structural characterization of the L0 cytoplasmic loop of human multidrug resistance protein 6 (MRP6)

Angela Ostuni*, Maria Antonietta Castiglione Morelli, Flavia Cuviello, Alfonso Bavoso, Faustino Bisaccia

Department of Sciences, University of Basilicata, viale Ateneo Lucano 10, Potenza 85100, Italy

ARTICLE INFO

Keywords:
MRP6
Cytoplasmic loop L0
Structure
Circular dichroism
Fluorescence
NMR

ABSTRACT

ABCC6 is a member of the C subfamily of ATP-binding cassette transporters whose mutations are correlated to *Pseudoxanthoma elasticum*, an autosomal recessive, progressive disorder characterized by ectopic mineralization and fragmentation of elastic fibers. Structural studies of the entire protein have been hindered by its large size, membrane association, and domain complexity. Studies previously performed have contributed to shed light on the structure and function of the nucleotide binding domains and of the N-terminal region. Here we report the expression in *E. coli* of the polypeptide E_{205}-G_{279} contained in the cytoplasmic L0 loop. For the first time structural studies in solution were performed. Far-UV CD spectra showed that L0 is structured, assuming predominantly α-helix in TFE solution and turns in phosphate buffer. Fluorescence spectra indicated some flexibility of the regions containing aromatic residues. ^{1}H NMR spectroscopy identified three helical regions separated by more flexible regions.

1. Introduction

The human protein MRP6, codified by the ABCC6 gene, belongs to the ABCC subfamily of ATP-binding cassette (ABC) transporters [1]. It is mainly expressed in liver and kidney, in particular at the basolateral surface of hepatocytes [2]. MRP6 is associated to low level resistance to agents such as etoposide, teniposide, doxorubicin and daunorubicin [3,4]. Mutations of ABCC6 gene are responsible for *Pseudoxanthoma elasticum* (PXE), an autosomal recessive, progressive disorder characterized by ectopic mineralization and fragmentation of elastic fibers in skin, eyes and vascular tissues [5–7]. ABCC6-silenced hepatoma cells (HepG2) adopted a characteristic gene expression profile, thus modifying the cell secretory phenotype up-regulating pro-mineralization factors, down-regulating anti-mineralization factors [8] and showing a senescent-like cell phenotype [9]. Moreover ABCC6 plays a role in the activation of the purinergic system [10].

From a structural point of view, ABC transporters are classified in short, half and long [11]. MRP6 is a “long” transporter because it is expressed as a single polypeptide chain where the core MRP structure (two transmembrane domains TMD1 and TMD2, and two cytoplasmic nucleotide binding domains NBD1 and NBD2) is connected through a cytoplasmic loop, indicated as L0, to an additional NH_2-terminal transmembrane domain, indicated as TMD0 [12,13]. There are seven ABCC transporters that contain the TMD0L0 region at the N terminus, and ABCC7 contains only the L0 loop but not TMD0. The N-terminal sequence of L0 is relatively conserved among the ABCC proteins including members that do not have TMD0 [14].

For many ABC transporters the core domain is sufficient for proper localization, ATP hydrolysis, and substrate recognition. The possible roles of the additional N-terminal region have been extensively studied only for few MRPs and indeed it may differ from one MRP protein to another. In MRP1, TMD0 is important for proper folding and retention in the plasma membrane [15] whereas L0 is required for proper trafficking and the transporter function [16,17] by interacting with glutathione [18]. In MRP2, TMD0 domain is important for trafficking and stabilization in the apical membrane [19] whereas L0 is essential for localization of the transporter [20]. TMD0 is important for activity of Sulfonylurea receptors, SUR1 and SUR2 (ABCC8 and ABCC9) and, together with L0, for the regulation of trafficking and gating of inwardly rectifying potassium channel Kir6.2 [21]. The lasso motif of cystic fibrosis transmembrane conductance regulator, CFTR, is involved in the membrane trafficking machinery and in channel gating (for references see [22]). Cryo-EM studies allowed to elucidate the structural basis of SUR1 [23], MRP1 [24] and CFTR [25].

Our previous studies have contributed to shed light on the structure and function of the NBDs [26–28] and of the N-terminal region of MRP6

* Corresponding author.
E-mail address: angela.ostuni@unibas.it (A. Ostuni).

https://doi.org/10.1016/j.bbamem.2018.11.002
Received 4 June 2018; Received in revised form 15 October 2018; Accepted 8 November 2018
Available online 10 November 2018

by allowing to suggest a complex role for these regions in physiological and pathological contexts [29]. In particular, by using domain deletion constructs of ABCC6, expressed in HEK293 and polarized LLC-PK1 cells, it has been suggested that L0 could play a role in the correct routing of both TMD0 and core domain [30].

Here we report the cytoplasmic L0 loop expression in *E. coli* and its structural study in solution by using circular dichroism, fluorescence and NMR spectroscopies.

2. Material and methods

2.1. Construction of expression vector

The E_{205}-G_{279} region of human MRP6 protein was selected following bioinformatics analysis since it represents the L0 sequence with greater homology with the same domain of other MRP proteins.

The polypeptide was amplified by PCR from the expression vector pcDNA3.1-Flag-ABCC6 [8] and cloned in pGEX-2T vector (GE Healthcare) using *Bam*HI and *Eco*RI restriction enzymes. The forward primer 5′-TCGCGGATCCGAGACTGGGGCAGCCTTCC-3′ and the reverse primer 5′-CGAGGTACCGAATTCTCAGCCACTGCCGCCTTTC-3′ were used. For amplification GoTaq® qPCR Master Mix (Promega) and 30 ng of template were used in a 25 μL reaction volume. PCR reaction mixture was subjected to an initial denaturation of 2 min at 95 °C, 30 cycles of 1 min denaturation at 95 °C, 1 min annealing at 59 °C and 30 s amplification at 72 °C and a final amplification step of 5 min at 72 °C. The PCR product was revealed on a 1.5% agarose gel and purified by QIAquick PCR purification kit (Qiagen).

L0 construct was designed as a fusion GST-tagged protein. The L0 fragment and the pGEX-2T expression vector (GE Healthcare Life Sciences) were digested with *Eco*RI (BioLabs) and *Bam*HI (BioLabs) restriction enzymes and then ligated. After ligation, One Shot Top Ten cells (Invitrogen) were transformed with the ligation product. The sequence and the correct orientation of the insert were confirmed by DNA sequencing (Eurofins Genomic, Germany).

2.2. Expression of the recombinant protein

The *E. coli* Rosetta pLYS-S (Novagen) cells were transformed with recombinant pGEXL0 vector and the transformed colonies were selected at 37 °C on Luria-Bertani agar plates containing 100 μg/mL ampicillin and 50 μg/mL chloramphenicol. A single colony was picked and grown in 10 mL of Luria-Bertani medium at 37 °C for 16 h with shaking and then were diluted 20-fold in M9 medium containing ^{15}N and micronutrients 1× ($(NH_4)_6Mo_7O_{24}{\cdot}4H_2O$, H_3BO_3, $CoCl_2{\cdot}6H_2O$, $CuSO_4{\cdot}5H_2O$, $MnCl_2{\cdot}4H_2O$ e $ZnSO_4{\cdot}7H_2O$). When OD600 reached 0.7–0.8, the transcription of the gene was induced by the addition of 2 mM isopropyl-thiogalactoside (IPTG) over night at 37 °C.

Cells harvested by centrifugation were lysed in PBS buffer by sonication (Bandelin sonicator) on ice. The soluble and the insoluble cell fractions were separated by centrifugation at 13000 rpm for 15 min at 4 °C and analyzed on 16%-4% Tricine-SDS-polyacrylamide gels. After electroblotting, PVDF membranes (Amersham Bioscience) were blocked for one hour in PBS-0.05% Tween 20 with 2% non-fat milk and incubated overnight at 4 °C with rabbit polyclonal anti-GST (dilution 1:10000; Sigma). Membranes were washed in PBS-T and incubated for one hour with horseradish peroxidase–conjugated anti-rabbit secondary antibody (dilution 1:10000; Sigma). Reactive proteins were revealed with Chemiluminescent Peroxidase Substrate (Sigma) and ChemiDoc™ MP System (Biorad).

2.3. Purification of L0 polypeptide

The insoluble fraction obtained after cell lyse was washed two times with Tris-EDTA buffer containing Triton (10 mM Tris-HCl pH 8, 1 mM EDTA, 0.5% Triton X-100) and resuspended with buffer (25 mM Tris pH 8, 75 mM NaCl, 0.05% β-mercaptoethanol) containing 0.1% sarcosyl. Samples were used for thrombin (THR) digestion at 25 °C for 16 h using 0.02 U THR/μg recombinant protein. The polypeptide was purified by SHIMATZU-HPLC on a C18 column (Jupiter 5 μm, 300A, 250 × 4.60 mm, Phenomenex) using a gradient of acetonitrile/water in 0.1% trifluoroacetic acid. To assess the purity of ^{15}N-labelled L0, MALDI TOF/MS spectra were acquired by a MALDI micro MX (Waters).

Protein concentration was determined by measuring the optical absorbance at 280 nm using 28,990 $M^{-1}\,cm^{-1}$ as extinction coefficient calculated from the amino acid composition [31].

2.4. Circular dichroism spectroscopy

CD spectra of L0 were acquired at 25 °C or at the temperature indicated with a Jasco J-815 CD Spectrometer with a light source constituted by a Xenon 250 W lamp and equipped with a thermoelectric temperature controller. The acquisition was carried out in a cylindrical quartz thermostated cell with an optical path of 0.1 cm in the spectral range 190–250 nm, a scanning speed of 100 nm/min, 1 nm bandwidth, a time-constant of 0.5 s, 20 mdeg of sensitivity and a total number of 16 accumulations for each spectrum. Then, the baseline spectra of the solvents were subtracted and spectra were smoothed using the Fourier transform. Spectra were recorded in sodium phosphate buffer (10 mM, pH 7.4) and in 20% and 80% 2,2,2-Trifluoroethanol (TFE), at the concentration of 15 μM. Data were expressed in terms of the molar ellipticity per residues in units of deg × cm^2 × $dmol^{-1}$. Analysis of CD spectra for the evaluation of secondary structure content was performed with DICHROWEB [32] using the CONTINLL algorithm with a data set protein that require a minimum range of 190–240 nm of the CD data [33,34]. Thermal denaturation of the secondary structure was followed by measuring the ellipticity changes at 222 nm with increasing temperatures in the range 5–75 °C; the sample was heated at a constant rate of 5 °C/min.

2.5. Intrinsic fluorescence measurements

The intrinsic tryptophan fluorescence of the polypeptide (15 μM) was measured in sodium phosphate buffer (10 mM, pH 7.4), 20% and 80% TFE. The experiment was performed at 25 °C on an Agilent Technologies Cary Eclipse Fluorescence Spectrophotometer. The excitation wavelength was set at 295 nm and emission was scanned over the range 300–420 nm with scan rate of 30 nm/min, averaging time 1 s and data interval 0.5 nm.

2.6. NMR spectroscopy

The sample for NMR was prepared as approximately 2 mM in H_2O/TFE-d_3 20:80 (v/v). The ^1H NMR spectra were acquired at 25 °C on a Varian Inova 500 spectrometer. A spectral width of 5900 Hz and pulse width of 7.4 μs (90°) were used. The water signal was suppressed by a 2.5-s pre-saturation pulse or with a *dpfgse* pulse sequence. One-dimensional spectra were acquired using 128 transients and 16 k data points which were zero filled to 65 k data points. Two-dimensional TOCSY and NOESY spectra (with mixing times of 65 and 80 ms and in the range 100–250 ms, respectively) were acquired in phase-sensitive mode using 2 k data points, 64 transients and 256 increments. Chemical shift were referenced to DSS (4,4-dimethyl-4-silapentane-1-sulfonic acid). The ^1H,^{15}N-HSQC experiment was recorded at 25 °C on a Bruker 600 MHz spectrometer at Institute of Biomolecular Chemistry, CNR, Pozzuoli.

2.7. Bioinformatics analysis

Secondary structure predictions and homology modeling were performed with the PredictProtein Server [35] and Phyre2 Server [36], respectively. Figures of the models were prepared with the molecular

graphics program MOLMOL [37].

3. Results and discussion

Analysis of the structures of MRP proteins allows to understand how they are oriented into the cell membranes, their transport mechanism, from ATP binding and hydrolysis to substrate binding and its translocation and finally, it allows to design possible drugs for modulating their activity. However, membrane proteins are relatively flexible and unstable, in the detergent micelles into which they must be extracted for purification, so it is difficult that they can be trapped in a particular conformation and therefore it is difficult to crystallize them [38]. Therefore, when there is very little or no production at all of the whole protein, individually domains are produced and their single structures are studied in solution. In order to shed light on the secondary and tertiary structure of the L0 loop of MRP6 we expressed the polypeptide in *E. coli*. Structural studies in solution using circular dichroism, fluorescence and NMR spectroscopies were performed.

3.1. Expression and purification

Gene coding for E_{205}-G_{279} region of human MRP6 protein was cloned in pQE30 vector to overproduce L0 in *E. coli* as an N-terminally His6-tagged polypeptide. Unfortunately, despite many attempts using different host bacteria (BL21, BL21DE3, Rosetta pLYS-S), growth temperatures, IPTG concentrations, induction times, or with the addition of glucose in the medium to control basal induction, polypeptide was expressed with a low yield and in inclusion bodies. Construction of the chimera L0 with an N-terminal GST-tag allowed us to obtain the best production yield into a Rosetta pLYS-S *E. coli* strain containing the pRARE plasmid encoding tRNAs for the rare codons of Arg, Ile, Leu and Pro.

As shown in Fig. 1A upon induction by 2 mM IPTG over night at 37 °C, as compared to the uninduced bacterial culture (lane 2), GST-L0 (38 kDa molecular weight) was expressed as major protein product (lane 4) within fraction of the insoluble proteins. L0 was properly cleaved from its tag using thrombin (lane 5) as confirmed by Western blot analysis (Fig. 1B). The expression of GST-L0 chimera was verified also at 25 °C but a poor yield was observed, and anyway, the protein was in inclusion bodies. Moreover, neither the use of other bacterial hosts (BL21, BL21DE3), nor different times of induction, nor different concentrations of IPTG avoided or at least reduced the formation of inclusion bodies.

Purification with RP-HPLC was carried out. The abundant peak was collected at 57% acetonitrile and mass spectrometry confirmed that this fraction (molecular weight of 8863 Da) corresponds to the polypeptide E_{205}-G_{279} with a glycine and a serine at the N-terminal: GSETGAAFPSKATFWWVSGLVWRGYRRPLRPKDLWSLGRENSSEELVSRLEKEWMRNRSAARRHNKAIAFKRKGGSG as expected after digestion with thrombin.

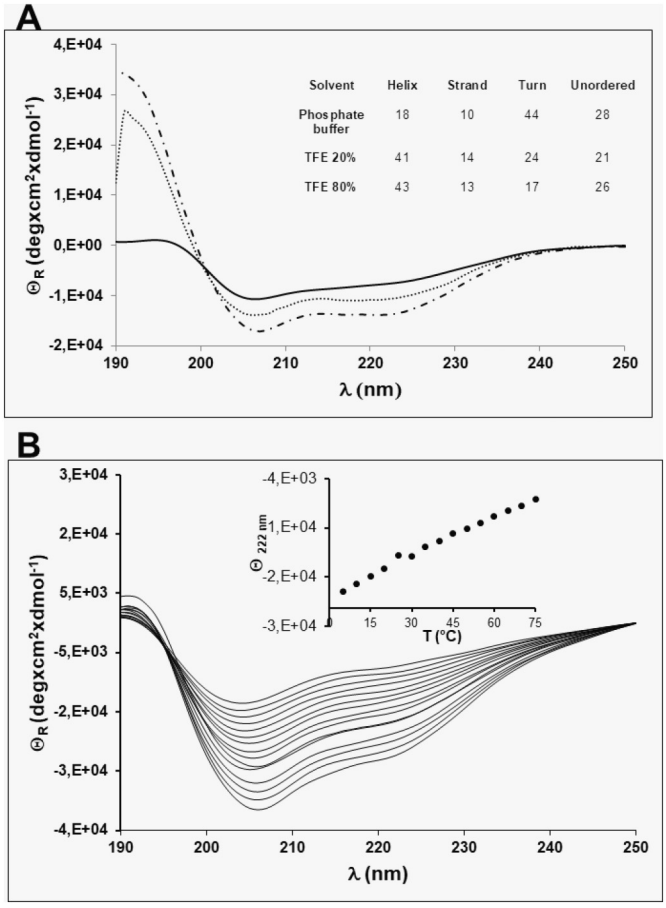

Fig. 2. Far-UV CD spectra of L0. (A) 10 mM sodium phosphate buffer pH 7.4 (—), 20% TFE (····) and 80% TFE (- - -). The inset shows the fractions of secondary structure estimated from the deconvoluted CD spectra by the CONTINLL algorithm. (B) CD spectra of 15 μM L0 in 80% TFE between 5 °C and 75 °C. The inset shows the ellipticity at 222 nm at different temperatures.

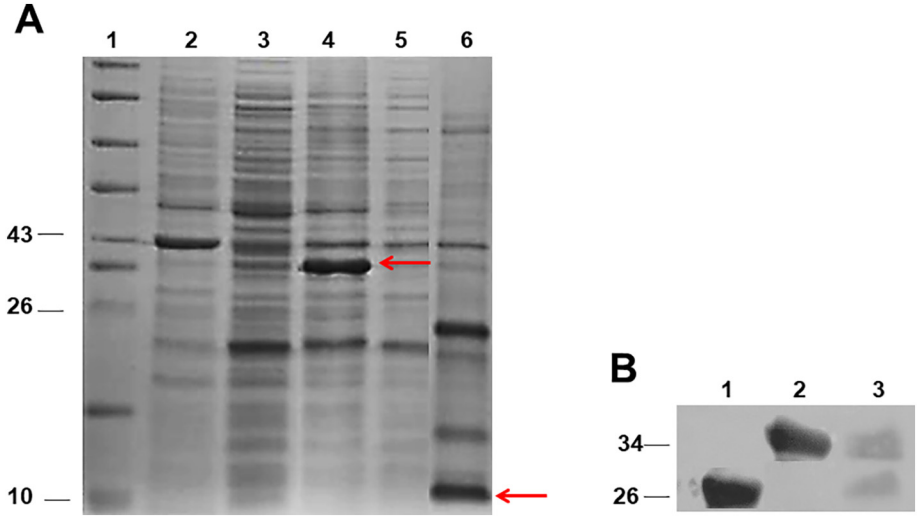

Fig. 1. Expression of L0. (A) The polypeptide was purified as described in the Material and methods section and was analyzed by SDS PAGE and Coomassie Blue staining. Lane 1: protein molecular-mass standards (KDa); lane 2: not soluble bacterial proteins before IPTG induction; lane 3: soluble bacterial proteins before IPTG induction; lane 4: not soluble proteins of IPTG-induced bacteria. A red arrow indicates GST-L0; lane 5: soluble proteins of IPTG-induced bacteria; lane 6: not soluble protein after thrombin digestion. A red arrow indicates L0. (B) Western immunoblotting with rabbit polyclonal anti-GST and horseradish peroxidase–conjugated anti-rabbit secondary antibody of (lane 1) not soluble protein after thrombin digestion and (lane 2) before thrombin digestion; protein molecular-mass standards (KDa) (lane 3).

3.2. Circular dichroism

Far UV CD spectra (190–250 nm) provide information on secondary structure of proteins [33,39]. Here we used CD spectroscopy for the preliminary evaluation of the conformation and stability of L0 in different environmental conditions. L0 contains about 60% of hydrophobic residues and it shows very low solubility in aqueous solutions so we used mixtures of water and TFE. TFE is an alcohol based cosolvent that has been largely used to promote native-like structures and to stabilize secondary structures of peptides in aqueous solutions [40]. Furthermore, the use of high concentrations of TFE has been popular in solubilizing peptides and proteins for studies by NMR spectroscopy [41].

In Fig. 2A are reported the CD spectra of L0 in phosphate buffer, in 20% and 80% TFE at a concentration of 15 μM. Evaluation of the secondary structure content performed with DICHROWEB software [32] showed that L0 is structured, assuming predominantly α-helix in TFE solution and turns in phosphate buffer.

Analysis of CD spectra of polypeptide as a function of temperature allowed to determine the thermodynamics of folding. Thermal induced conformational variation was monitored by changes of the ellipticity at 222 nm which is proportional to the α-helical content. CD spectra were run in the temperature range 5 °C–75 °C in 80% TFE where L0 showed greater solubility (Fig. 2B).

An isodichroic point was observed near 200 nm suggesting an equilibrium between two conformational states, α-helix and random coil [42]. L0 has a higher content of α-helix between 30 and 50 °C (50%), while at 10 °C it shows a higher content of strand (38%) and random coil (40%) up to 25 °C. The inset of Fig. 2B shows, a linear increase of the ellipticity at 222 nm with temperature. This indicates a tendency of the polypeptide to structurally stabilize α-helixes.

3.3. Fluorescence spectroscopy measurements

The tertiary structural changes in different solvent media were monitored by the intrinsic fluorescence spectra. In the native folded state, tryptophans and tyrosines are generally located within the core of the protein, whereas in a partially folded or unfolded state they become exposed to solvent. Protein folding monitored by tryptophan fluorescence excitation is advantageous due to its higher quantum yield, longer excited-state lifetime, and sensitivity of its fluorescence to the environment [43].

Due to the presence of W217, W218, W224, W237, W256, fluorescence spectra (measured between 300 and 420 nm) of E_{205}-G_{279} polypeptide, solubilized at the same concentration of CD measurements, have been recorded (Fig. 3).

Fluorescence spectra of polypeptide showed higher fluorescence intensity in phosphate buffer with a maximum at 343 nm; in 20% and 80% TFE fluorescence intensity decreases and the maximum shifts to 353 nm. These results indicate that in TFE solution the aromatic residues are fully solvent exposed (“red shift”) with a consequently decrease in quantum yield. Anyway, the resulting fluorescence signal is averaged among all tryptophan residues which are exposed to a more or less hydrophobic environment as a result of their positions in folded or disordered structures, respectively.

3.4. NMR spectroscopy

To determine the three-dimensional structure of L0 NMR studies were performed in 80% TFE-d_3. These were the best conditions for solubilization and structuring suggested by the previously reported CD studies. The overall rather good chemical shift dispersion in ^{1}H spectra were suggestive of a quite folded protein. However, the ^{1}H, ^{15}N-HSQC spectrum of L0 presented a lower number of NH-α cross peaks than expected; this was considered as indicative of a not completely ordered protein, at least in the used experimental conditions.

Partial resonance assignments of proton chemical shifts of L0 were obtained by interpretation of the two-dimensional TOCSY and NOESY spectra at 25 °C, according to standard methods [44]. The assignment of the spin systems was obtained for 48 out of 75 amino acids of L0 (64%), most of these residues belonged to regions of L0 with regular secondary structures. Three helical regions were identified by the observation of characteristic sequential and medium range NOE connectivities (Fig. 4).

In the regions between residues: S212 and G226, L248 and A262, K268 and K273 we observed strong dNN sequential connectivities together with numerous $daN_{(i,\ i+3)}$, $da\beta_{(i,\ i+3)}$, all characteristic of helical regions. However, due to quite severe overlaps of αH and NH chemical shifts in other regions, many sequential connectivities for residues in more flexible regions could not be unambiguously assigned.

The method of Wishart et al. (1992) [45] was used for corroborating the assessment of L0 secondary structure. The Chemical Shift Index method is based on changes in the CHα proton chemical shifts when the amino acids are in a well-defined secondary structure. In particular, an α-helical structure is identified by four or more consecutive negative secondary shifts (with a high-field shift relative to the corresponding random coil values) while a β-strand is identified by three or more consecutive positive secondary shifts (low-field shift relative to the corresponding random coil values). The results for the analysis of the CHα proton chemical shifts for L0 in 80% TFE-d_3 show that for the above-mentioned residues the difference in the chemical shifts is continually negative, which confirms that helical secondary structures are present in these regions.

In summary, due to unfavorable overlapping resonances and only a partial resonance assignment, a more detailed structural characterization of the region E_{205}-G_{279} of L0 was not possible by NMR. Hence, in order to assess the polypeptide global conformation we resorted to bioinformatics analysis.

3.5. Bioinformatics analysis

Secondary structure prediction of the region E_{205}-G_{279} of L0 was obtained by the PredictProtein Server (http://www.predictprotein.org/). PredictProtein is an automatic service that searches up-to-date public sequence databases, creates alignments, and predicts various aspects of protein structure and function [35]. In our case, 49 aligned proteins were used for structure prediction and, among them, two PDB structures were matched, corresponding to the cryo-EM structures of bovine multidrug resistance protein 1 (MRP1) in an apo form and bound to leukotriene C4 [24] (PDB entry: 5UJ9). The E_{205}-G_{279} polypeptide was predicted to have 53.3% alpha helical structure and the remaining 46.7% is disordered. Three helical structures were predicted in the regions: S212-R225, S245-A262 and K268-K275. This prediction is in good agreement with the NMR findings where helices spanning residues S212-G226, L248-A262, K268-K273 were found.

Structural homology models for the region E_{205}-G_{279} of L0 were built with Phyre2 server (http://www.sbg.bio.ic.ac.uk/phyre2/html/page.cgi?id=index). The best model is based on template 5uj9A, corresponding to the two already cited structures of MRP1 [24], where MRP1 shares 45% amino acid sequence identity with MRP6. In this model 58 out of 75 residues of L0, from E205 to A262, corresponding to 76% of the whole sequence, were modeled with 99.7% homology confidence. This close homology model is represented in Fig. 5A,B. The side chains of tryptophan residues are shown in Fig. 5B: only W224 and W256 are in helical regions while W217, W218 and W237 are in flexible regions, thus confirming fluorescence results of different environments in which tryptophans may be possibly located.

Another 99.7% confidence model was calculated on template 5uakA, corresponding to the cryo-EM structure at 3.9 Å resolution of human CFTR [46] (PDB entry: 5UAK). In this model 73 residues of L0, from E205 to K275, corresponding to 96% of the whole sequence, were modeled. In spite of the lower amino acid sequence identity of CFTR with MRP6 (26%), the C-terminal helix of L0 found by NMR was also

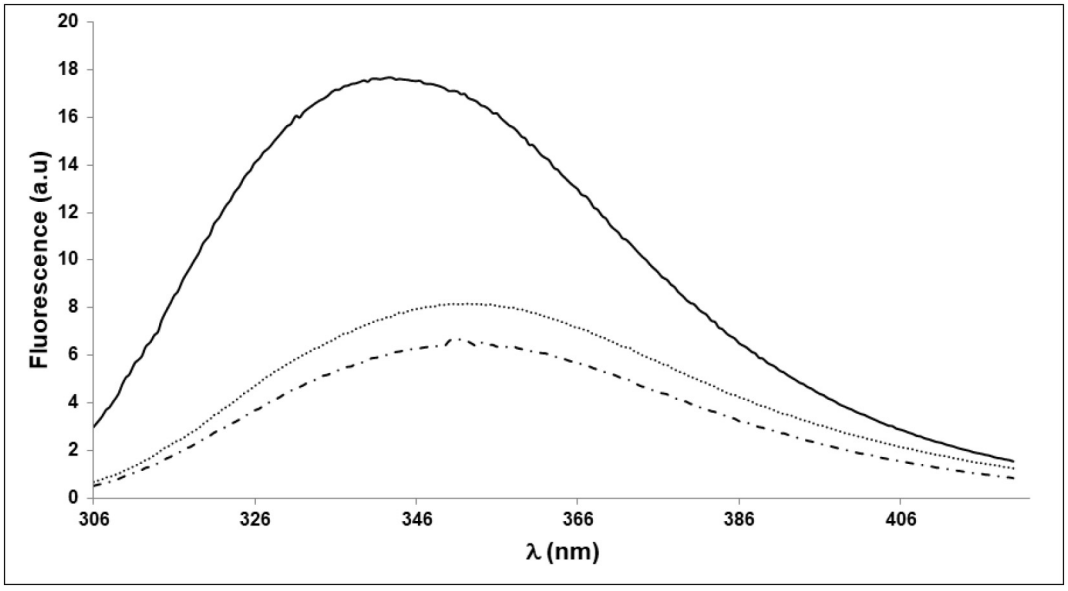

Fig. 3. Fluorescence emission spectra of L0. The polypeptide (15 μM) was dissolved in 10 mM sodium phosphate buffer pH 7.4 (—), 20% (·····) and 80% TFE (- - -). The solutions were allowed to stand at 25 °C for 10 min before fluorescence measurements with an excitation wavelength of 295 nm.

Fig. 4. Sequential and medium-range NOE connectivities and CSI index of CHα protons (Wishart et al., 1992). NOE connectivities are specified using the notation for the corresponding proton-proton distances (Wüthrich, 1986). The height of each bar is approximately proportional to the strength of the corresponding NOE enhancement.

modeled (Fig. 5C).

In addition, residues E205-K275 of L0 were modeled on template 5ykeB, corresponding to the cryo-EM structure at 4.1 Å resolution of SUR1 in pancreatic ATP-sensitive potassium channels [47] (PDB entry: 5YKE). This model had a slightly higher confidence (99.8%) but the amino acid sequence identity with MRP6 is only 15% (Fig. 5D).

All models were obtained with Phyre2 server (Kelley et al., 2015).

4. Conclusions

With the aim to structurally characterize the L0 loop of human MRP6, in the present work we have produced the polypeptide E_{205}-G_{279}. Structural studies in solution by circular dichroism, fluorescence spectroscopy and NMR indicated the presence of three helices separated by more flexible segments, both regions containing aromatic residues.

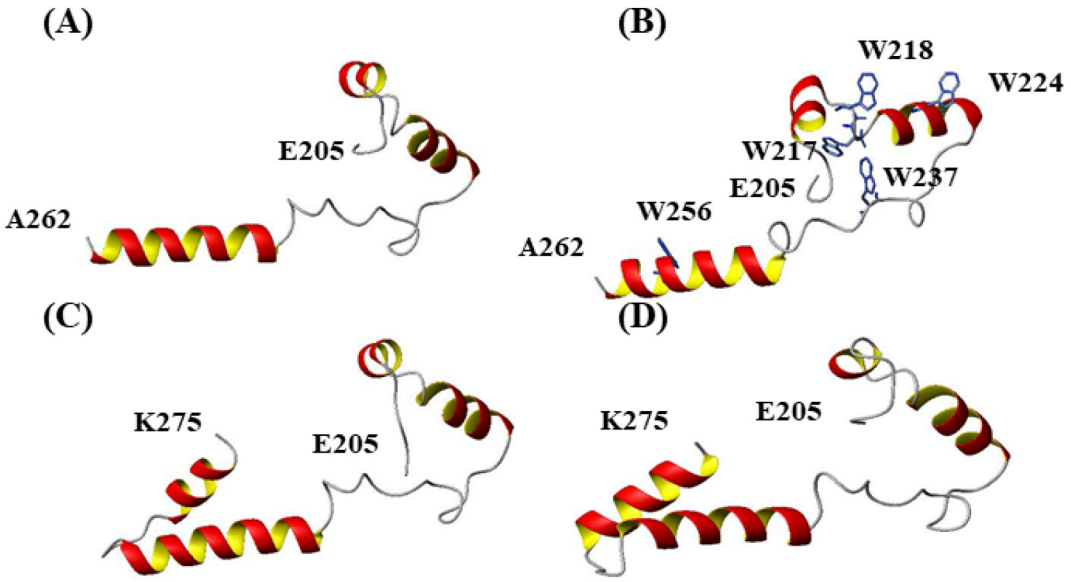

Fig. 5. Cartoon representations of homology models of L0 loop: (A) residues E_{205}-A_{262}. The PDB structure 5UJ9, corresponding to **MRP1**, was used as template; (B) another view of the model reported in (A) with the side chains of tryptophan residues shown in stick representation; (C) residues E_{205}-K_{275}. The PDB structure 5UAK, corresponding to **CFTR**, was used as template; (D) residues E_{205}-K_{275}. The PDB structure 5YKE, corresponding to **SUR1**, was used as template.

The *in silico* results were in agreement with experimental observations. The structural homology of MRP6-L0 with the corresponding domain of other MRPs is an agreement with the common role for plasma membrane localization.

All considered these findings lay the basis for future exploration of structure-function correlations taking also into account that human MRP6-L0 region contains some amino acid residues that are mutated in PXE [48]. In addition, future interactomics studies with the region E_{205}-G_{279} might help in revealing the partner proteins of MRP6.

Conflict of interest

The authors confirm that this article content has no conflict of interest.

Transparency document

The Transparency document associated with this article can be found, in online version.

Acknowledgments

The authors thank Dr. Antonio Vassallo for the mass spectra of L0 and Dr. Andrea Motta (Institute of Biomolecular Chemistry, CNR, Pozzuoli, Italy) for the ^{1}H,^{15}N-HSQC spectra.

References

[1] C. Thomas, R. Tampé, Multifaceted structures and mechanisms of ABC transport systems in health and disease, Curr. Opin. Struct. Biol. 51 (2018) 116–128, https://doi.org/10.1016/j.sbi.2018.03.016.
[2] G.L. Scheffer, X. Hu, A.C. Pijnenborg, J. Wijnholds, A.A. Bergen, R.J. Scheper, MRP6 (ABCC6) detection in normal human tissues and tumors, Lab. Investig. 82 (2002) 515–518.
[3] R.G. Deeley, C. Westlake, S.P. Cole, Transmembrane transport of endo- and xenobiotics by mammalian ATP-binding cassette multidrug resistance proteins, Physiol. Rev. 86 (2006) 849–899, https://doi.org/10.1152/physrev.00035.2005.
[4] A.M. Salvia, F. Cuviello, S. Coluzzi, R. Nuccorini, I. Attolico, S.P. Pascale, F. Bisaccia, M. Pizzuti, A. Ostuni, Expression of some ATP-binding cassette transporters in acute myeloid leukemia, Hematol. Rep. 9 (7406) (2017) 137–141, https://doi.org/10.4081/hr.2017.7406.
[5] G. Favre, A. Laurain, T. Aranyi, F. Szeri, K. Fulop, O. Le Saux, C. Duranton, G. Kauffenstein, L. Martin, G. Lefthériotis, The ABCC6 transporter: a new player in biomineralization, Int. J. Mol. Sci. 18 (2017) 1941, https://doi.org/10.3390/ijms18091941.
[6] K. Moitra, S. Garcia, M. Jaldin, C. Etoundi, D. Cooper, A. Roland, P. Dixon, S. Reyes, S. Turan, S. Terry, M. Dean, ABCC6 and pseudoxanthoma elasticum: the face of a rare disease from genetics to advocacy, Int. J. Mol. Sci. 18 (2017) 1488, https://doi.org/10.3390/ijms18071488.
[7] R.S. Jansen, S. Duijst, S. Mahakena, D. Sommer, F. Szeri, A. Váradi, A. Plomp, A.A. Bergen, R.P. Oude Elferink, P. Borst, K. van de Wetering, ABCC6-mediated ATP secretion by the liver is the main source of the mineralization inhibitor inorganic pyrophosphate in the systemic circulation-brief report, Arterioscler. Thromb. Vasc. Biol. 34 (2014) 1985–1989, https://doi.org/10.1161/ATVBAHA.114.304017.
[8] R. Miglionico, M.F. Armentano, M. Carmosino, A.M. Salvia, F. Cuviello, F. Bisaccia, A. Ostuni, Dysregulation of gene expression in ABCC6 knockdown HepG2 cells, Cell. Mol. Biol. Lett. 19 (2014) 517–526, https://doi.org/10.2478/s11658-014-0208-2.
[9] R. Miglionico, A. Ostuni, M.F. Armentano, L. Milella, E. Crescenzi, M. Carmosino, F. Bisaccia, ABCC6 knockdown in HepG2 cells induces a senescent-like cell phenotype, Cell. Mol. Biol. Lett. 22 (2017) 7, , https://doi.org/10.1186/s11658-017-0036-2.
[10] F. Martinelli, F. Cuviello, M.C. Pace, M.F. Armentano, R. Miglionico, A. Ostuni, F. Bisaccia, Extracellular ATP regulates CD73 and ABCC6 expression in HepG2 cells, Front. Mol. Biosci. 5 (2018) 75 (eCollection 2018), https://doi.org/10.3389/fmolb.2018.00075.
[11] A.J. Slot, S.V. Molinski, S.P. Cole, Mammalian multidrug-resistance proteins (MRPs), Essays Biochem. 50 (2011) 179–207, https://doi.org/10.1042/bse0500179.
[12] H. Lee, P. Lara, A. Ostuni, J. Presto, J. Johansson, I. Nilsson, H. Kim, Live-cell topology assessment of URG7, MRP6 and SP-C using glycosylatable green fluorescent protein in mammalian cells, Biochem. Biophys. Res. Commun. 450 (2014) 1587–1592, https://doi.org/10.1016/j.bbrc.2014.07.046.
[13] A. Ostuni, P. Lara, M.F. Armentano, R. Miglionico, A.M. Salvia, M. Mönnich, M. Carmosino, F.M. Lasorsa, M. Monné, I. Nilsson, F. Bisaccia, The hepatitis B x antigen anti-apoptotic effector URG7 is localized to the endoplasmic reticulum membrane, FEBS Lett. 587 (2013) 3058–3062, https://doi.org/10.1016/j.febslet.2013.07.042.
[14] C.J. Westlake, Y.M. Qian, M. Gao, M. Vasa, S.P. Cole, R.G. Deeley, Identification of the structural and functional boundaries of the multidrug resistance protein 1 cytoplasmic loop 3, Biochemistry 42 (2003) 14099–14113.
[15] C.J. Westlake, S.P. Cole, R.G. Deeley, Role of the NH2-terminal membrane spanning domain of multidrug resistance protein 1/ABCC1 in protein processing and trafficking, Mol. Biol. Cell 16 (2005) 2483–2492, https://doi.org/10.1091/mbc.e04-12-1113.
[16] E. Bakos, R. Evers, G. Calenda, G.E. Tusnády, G. Szakács, A. Váradi, B. Sarkadi, Characterization of the amino-terminal regions in the human multidrug resistance protein (MRP1), J. Cell Sci. 113 (2000) 4451–4461.
[17] Y.M. Qian, W. Qiu, M. Gao, C.J. Westlake, S.P. Cole, R.G. Deeley, Characterization of binding of leukotriene C4 by human multidrug resistance protein 1: evidence of differential interactions with NH2- and COOH-proximal halves of the protein, J. Biol. Chem. 276 (2001) 38636–38644, https://doi.org/10.1074/jbc.M107025200.
[18] X.Q. Ren, T. Furukawa, S. Aoki, T. Nakajima, T. Sumizawa, M. Haraguchi, Z.S. Chen, M. Kobayashi, S. Akiyama, Glutathione-dependent binding of a photoaffinity analog of agosterol A to the C-terminal half of human multidrug resistance protein, J. Biol. Chem. 276 (2001) 23197–23206, https://doi.org/10.1074/jbc.M101554200.

[19] S. Fernández, Z. Holló, A. Kern, É. Bakos, Role of the N-terminal transmembrane region of the multidrug resistance protein MRP2 in routing to the apical membrane in MDCKII cells, J. Biol. Chem. 277 (2002) 31048–31055, https://doi.org/10.1074/jbc.M204267200.
[20] P.E. Bandler, C.J. Westlake, C.E. Grant, S.P. Cole, R.G. Deeley, Identification of regions required for apical membrane localization of human multidrug resistance protein 2, Mol. Pharmacol. 74 (2008) 9–19, https://doi.org/10.1124/mol.108.045674.
[21] M. Winkler, P. Kühner, U. Russ, D. Ortiz, J. Bryan, U. Quast, Role of the amino-terminal transmembrane domain of sulfonylurea receptor SUR2B for coupling to K(IR)6.2, ligand binding, and oligomerization, Naunyn Schmiedeberg's Arch. Pharmacol. 385 (2012) 287–298.
[22] Z. Zhang, J. Chen, Atomic structure of the cystic fibrosis transmembrane conductance regulator, Cell 167 (2016) 1586–1597, https://doi.org/10.1007/s00210-011-0708-9.
[23] G.M. Martin, C. Yoshioka, E.A. Rex, J.F. Fay, Q. Xie, M.R. Whorton, J.Z. Chen, S.-L. Shyng, Cryo-EM structure of the ATP-sensitive potassium channel illuminates mechanisms of assembly and gating, elife 6 (2017) e24149, , https://doi.org/10.7554/eLife.24149.
[24] Z.L. Johnson, J. Chen, Structural basis of substrate recognition by the multidrug resistance protein MRP1, Cell 168 (2017) 1075–1085, https://doi.org/10.1016/j.cell.2017.01.041.
[25] B. Hoffmann, A. Elbahnsi, P. Lehn, J.L. Décout, F. Pietrucci, J.P. Mornon, I. Callebaut, Combining theoretical and experimental data to decipher CFTR 3D structures and functions, Cell. Mol. Life Sci. (2018), https://doi.org/10.1007/s00018-018-2835-7.
[26] A. Ostuni, R. Miglionico, F. Bisaccia, M.A. Castiglione Morelli, Biochemical characterization and NMR study of the region E748-A785 of the human protein MRP6/ABCC6, Protein Pept. Lett. 17 (2010) 861–866.
[27] A. Ostuni, R. Miglionico, M.A. Castiglione Morelli, F. Bisaccia, Study of the nucleotide-binding domain 1 of the human transporter protein MRP6, Protein Pept. Lett. 17 (2010) 1553–1558.
[28] A. Ostuni, R. Miglionico, M. Monné, M.A. Castiglione Morelli, F. Bisaccia, The nucleotide-binding domain 2 of the human transporter protein MRP6, J. Bioenerg. Biomembr. 43 (2011) 465–471, https://doi.org/10.1007/s10863-011-9372-5.
[29] F. Cuviello, Å. Tellgren-Roth, P. Lara, F. Ruud Selin, M. Monné, F. Bisaccia, I. Nilsson, A. Ostuni, Membrane insertion and topology of the amino-terminal domain TMD0 of multidrug-resistance associated protein 6 (MRP6), FEBS Lett. 589 (2015) 3921–3928, https://doi.org/10.1016/j.febslet.2015.10.030.
[30] R. Miglionico, A. Gerbino, A. Ostuni, M.F. Armentano, M. Monnè, M. Carmosino, F. Bisaccia, New insights into the roles of the N-terminal region of the ABCC6 transporter, J. Bioenerg. Biomembr. 48 (2016) 259–267, https://doi.org/10.1007/s10863-016-9654-z.
[31] P. Artimo, M. Jonnalagedda, K. Arnold, D. Baratin, G. Csardi, E. de Castro, S. Duvaud, V. Flegel, A. Fortier, E. Gasteiger, A. Grosdidier, C. Hernandez, V. Ioannidis, D. Kuznetsov, R. Liechti, S. Moretti, K. Mostaguir, N. Redaschi, G. Rossier, I. Xenarios, H. Stockinger, ExPASy: SIB bioinformatics resource portal, Nucleic Acids Res. 40 (2012) W597–W603, https://doi.org/10.1093/nar/gks400.
[32] L. Whitmore, B.A. Wallace, Protein secondary structure analyses from circular dichroism spectroscopy: methods and reference databases, Biopolymers 89 (2008) 392–400, https://doi.org/10.1002/bip.20853.
[33] S.W. Provencher, J. Glockner, Estimation of globular protein secondary structure from circular dichroism, Biochemistry 20 (1981) 33–37.
[34] I.H. van Stokkum, H.J. Spoelder, M. Bloemendal, R. van Grondelle, F.C. Groen, Estimation of protein secondary structure and error analysis from circular dichroism spectra, Anal. Biochem. 191 (1990) 110–118.
[35] B. Rost, G. Yachdav, J. Liu, The PredictProtein server, Nucleic Acids Res. 32 (2004) 321–326, https://doi.org/10.1093/nar/gkh377.
[36] L.A. Kelley, S. Mezulis, C.M. Yates, M.N. Wass, M.J.E. Sternberg, The Phyre2 web portal for protein modeling, prediction and analysis, Nat. Protoc. 10 (2015) 845–858, https://doi.org/10.1038/nprot.2015.053.
[37] R. Koradi, M. Billeter, K. Wüthrich, MOLMOL: a program for display and analysis of molecular structures, J. Mol. Graph. 14 (1996) 51–55.
[38] K.R. Vinothkumar, R. Henderson, Structures of membrane proteins, Q. Rev. Biophys. 43 (2010) 65–158, https://doi.org/10.1017/S0033583510000041.
[39] D.H.A. Corrêa, C.H.I. Ramos, The use of circular dichroism spectroscopy to study protein folding, form and function, Afr. J. Biochem. Res. 3 (2009) 164–173.
[40] D. Roccatano, G. Colombo, M. Fioroni, A.E. Mark, Mechanism by which 2,2,2-trifluoroethanol/water mixtures stabilize secondary-structure formation in peptides: a molecular dynamics study, Proc. Natl. Acad. Sci. U. S. A. 99 (2002) 12179–12184, https://doi.org/10.1073/pnas.182199699.
[41] M. Buck, Trifluoroethanol and colleagues: cosolvents come of age. Recent studies with peptides and proteins, Q. Rev. Biophys. 31 (1998) 297–355.
[42] M.E. Holtzer, A. Holtzer, Alpha-helix to random coil transitions: determination of peptide concentration from the CD at the isodichroic point, Biopolymers 32 (1992) 1675–1677, https://doi.org/10.1002/bip.360321209.
[43] Y.K. Reshetnyak, Y. Koshevnick, E.A. Burstein, Decomposition of protein tryptophan fluorescence spectra into log-normal components. III. Correlation between fluorescence and microenvironment parameters of individual tryptophan residues, Biophys. J. 81 (2001) 1735–1758, https://doi.org/10.1016/S0006-3495(01)75825-0.
[44] K. Wüthrich, NMR of Proteins and Nucleic Acids, Wiley & Sons, New York, 1986.
[45] D.S. Wishart, B.D. Sykes, F.M. Richards, The chemical shift index: a fast and simple method for the assignment of protein secondary structure through NMR spectroscopy, Biochemistry 31 (1992) 1647–1651.
[46] F. Liu, Z. Zhang, L. Csanády, D.C. Gadsby, J. Chen, Molecular structure of the human CFTR ion channel, Cell 169 (2017) 85–95, https://doi.org/10.1016/j.cell.2017.02.024.
[47] J.X. Wu, D. Ding, M. Wang, Y. Kang, X. Zeng, L. Chen, Ligand binding and conformational changes of SUR1 subunit in pancreatic ATP-sensitive potassium channels, Protein Cell 9 (2018) 553–567, https://doi.org/10.1007/s13238-018-0530-y.
[48] A.S. Plomp, R.J. Florijn, J. ten Brink, B. Castle, H. Kingston, A.M. Santiago, T.G.M.F. Gorgels, P.T.V.M. De Jong, A.A.B. Bergen, *ABCC6* mutations in pseudoxanthoma elasticum: an update including eight novel ones, Mol. Vis. 14 (2008) 118–124.